hydrogen

MDPI

Article

Methods to Improve the First Hydrogenation of the Vanadium-Rich BCC Alloy $Ti_{16}V_{60}Cr_{24}$

Francia Ravalison [1], Eugen Rabkin [2] and Jacques Huot [1,*]

[1] Hydrogen Research Institute, Université du Québec à Trois-Rivières, 3351 Des Forges, Three Rivers, QC G9A 5H7, Canada; francia.ravalison@irh.ca
[2] Department of Materials Science and Engineering, Technion-Israel Institute of Technology, Technion City, Haifa 3200003, Israel; erabkin@technion.ac.il
* Correspondence: jacques.huot@irh.ca; Tel.: +1-819-376-5011 (ext. 3576)

Abstract: In this paper we report the effect of three different preparation methods on the first hydrogenation of the vanadium-rich BCC alloy $Ti_{16}V_{60}Cr_{24}$: one-time cold rolling, 5 min ball milling and addition of 4 wt.% of Zr. All samples were synthesized by arc melting. Without Zr addition the alloy was single phase, but when 4 wt.% Zr was added, a secondary zirconium-rich phase was present. However, X-ray diffraction patterns only showed a single-body-centred cubic phase before hydrogenation for all samples. The crystal structure of the fully hydrogenated samples was body-centred tetragonal. The highest hydrogen capacity (3.8 wt.%) was measured for the Zr-doped alloy. The ball-milled alloy also exhibited a high storage capacity and fast kinetics. However, the maximum hydrogen storage capacity slightly decreased after cold rolling. It was found that air exposure increases incubation time for the first hydrogenation. The incubation time was shortened by cold rolling which, however, reduced the hydrogen storage capacity. The Pressure-Composition isotherms of $Ti_{16}V_{60}Cr_{24}$ + 4 wt.% Zr at 297, 303 and 323 K were determined. The determined enthalpy and entropy of hydrides formation were -41 ± 5 kJ/mol and -134 ± 14 J/mol/K, respectively.

Keywords: BCC alloys; ball milling; cold rolling; kinetics; hydrogen storage; thermodynamics

Citation: Ravalison, F.; Rabkin, E.; Huot, J. Methods to Improve the First Hydrogenation of the Vanadium-Rich BCC Alloy $Ti_{16}V_{60}Cr_{24}$. *Hydrogen* **2022**, *3*, 303–311. https://doi.org/10.3390/hydrogen3030018

Academic Editor: Maurizio Peruzzini

Received: 23 June 2022
Accepted: 21 July 2022
Published: 22 July 2022

1. Introduction

Vanadium-based body centred cubic (BCC) alloys are interesting materials for hydrogen storage because of their relatively high gravimetric storage capacity (~4 wt.%) and fast hydrogenation-dehydrogenation kinetics at room temperature [1–5]. However, the first hydrogenation (the so-called activation) is slow and usually necessitates high pressure/temperature [6]. Heat treatment is usually required before the first hydrogenation. This annealing results in good homogeneity, which is claimed to result in better hydrogen sorption properties [7–9]. Since this method is expensive for industrial production, investigations have been carried out to find alternatives. Techniques such as alloying with additives [10–12] and mechanical processing [13–16] have been found to improve the hydriding/dehydriding of vanadium based BCC alloys.

The addition of Zr in a Ti-V-Cr system leads to the formation of a secondary phase that acts as a gateway for hydrogen [17–19]. An amount of 4 wt.% of Zr seems to be the optimum for obtaining a high capacity and fast kinetics. Higher Zr content results in faster kinetic but decreases the hydrogen storage capacity [20]. Additionally, mechanical processing such as cold rolling and ball milling create defects that change the kinetics of hydrogen absorption/desorption. For example, one-time cold rolling or ball milling for 5 min drastically shortens the activation time [14]. As there are many ways to improve the first hydrogenation, it is interesting to compare them in order to see which one is the most efficient. For this investigation, the BCC alloy $Ti_{16}V_{60}Cr_{24}$ was selected. The effect of Zr addition and mechanical deformations by cold rolling or ball milling on the first

hydrogenation were studied. We further examined the effect of air exposure on the first hydrogenation and how mechanical deformation could regenerate the alloy.

2. Materials and Methods

All elements were purchased from Alfa-Aesar (Tewksbury, MA, USA) and had the following purities: Ti (99.95%), V (99%), Cr (99%) and Zr (99.95%). The alloys (~3 g each) were prepared by arc melting under argon atmosphere. Each pellet was melted, turned over and melted again three times to ensure homogeneity. The pellet was then hand-crushed using a hardened steel mortar and pestle in an argon-filled glove box.

Cold rolling was performed with a Durston DRM 130 (High Wycombe, UK) by inserting the hand-crushed powder between two 316 stainless steel plates. Ball milling was carried out on a Spex 8000 high-energy ball (SPEX Sample Prep, Metuchen, NJ, USA) in a hardened 55 cc steel crucible and balls (powder/ball mass ratio was 1/10).

Hydrogenation was performed at room temperature under 30 bars of hydrogen pressure using a homemade Sievert's apparatus. After full absorption, the desorption pressure–composition isotherms (PCI) were determined at 297, 303 and 323 K. For the kinetics measurements, the reactor was first vacuumed for about 1 h. Thereafter, hydrogen gas at a pressure of 30 bar was rapidly introduced into the reactor. The change of pressure with time gives the amount of hydrogen absorbed by the sample. For the determination of entropy and enthalpy from the Van't Hoff plot, the equilibrium pressure at mid-range was selected for each isotherm. In the present case, it means the equilibrium pressure was at a capacity of 0.75 wt.%. Morphology was studied using Hitachi Su1510 scanning electron microscope (Hitachi High-Tech Canada, Inc., Toronto, ON, Canada). Crystal structures before and after hydrogenation were investigated with a Bruker D8 Focus X-ray diffractometer (Madison, WI, USA) using the Cu Kα radiation. Crystal structure parameters were then evaluated from Rietveld refinement using Topas software (Bruker, Madison, WI, USA) [21].

3. Results

3.1. Microstructure

Figure 1 shows the backscattered electron micrographs of as-cast $Ti_{16}V_{60}Cr_{24}$ and $Ti_{16}V_{60}Cr_{24}$ + 4 wt.% Zr alloys.

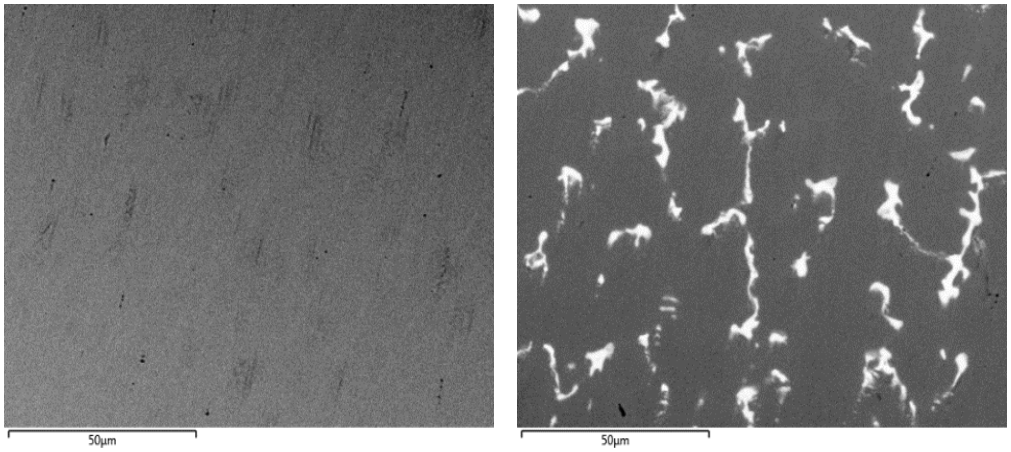

(**a**) (**b**)

Figure 1. Backscattered electron micrographs of as-cast (**a**) $Ti_{16}V_{60}Cr_{24}$ alloy; (**b**) $Ti_{16}V_{60}Cr_{24}$ + 4 wt.% Zr alloy.

One can notice that the alloy without Zr addition is single phase while the one with zirconium is made up of two phases: a matrix (grey) and a secondary phase (bright). Using Image J software (Wayne Rasband, National Institute of Mental Health, Bethesda, MD, USA) the area fraction of the bright phase is found to be around 7%.

From EDX bulk measurement, it was confirmed that the composition of the of $Ti_{16}V_{60}Cr_{24}$ alloy was close to the nominal one. In the case of $Ti_{16}V_{60}Cr_{24}$ + 4 wt.% Zr, the average elemental composition of each phase is presented in Table 1. In the matrix phase, the concentrations of Ti, V and Cr are relatively close to the nominal values, but very small for zirconium. The zirconium is essentially found in the bright phase. It is known that titanium is totally miscible in zirconium while chromium and vanadium solubility in zirconium are small [22]. This may be the reason why the concentration of titanium is high in the bright phase, while the concentrations of vanadium and chromium are low.

Table 1. EDX analysis showing the elemental composition of phases of $Ti_{16}V_{60}Cr_{24}$ + 4 wt.% Zr alloy.

Element	Matrix Phase	Bright Phase
Ti	14.2	33.8
V	62.4	5.1
Cr	22.9	1.8
Zr	0.5	59.3

Figure 2 represents the micrographs of the cold-rolled (a) and the ball-milled (b) $Ti_{16}V_{60}Cr_{24}$ alloys. Cold rolling leads to the formation of a plate, whereas ball milling results in fine powder.

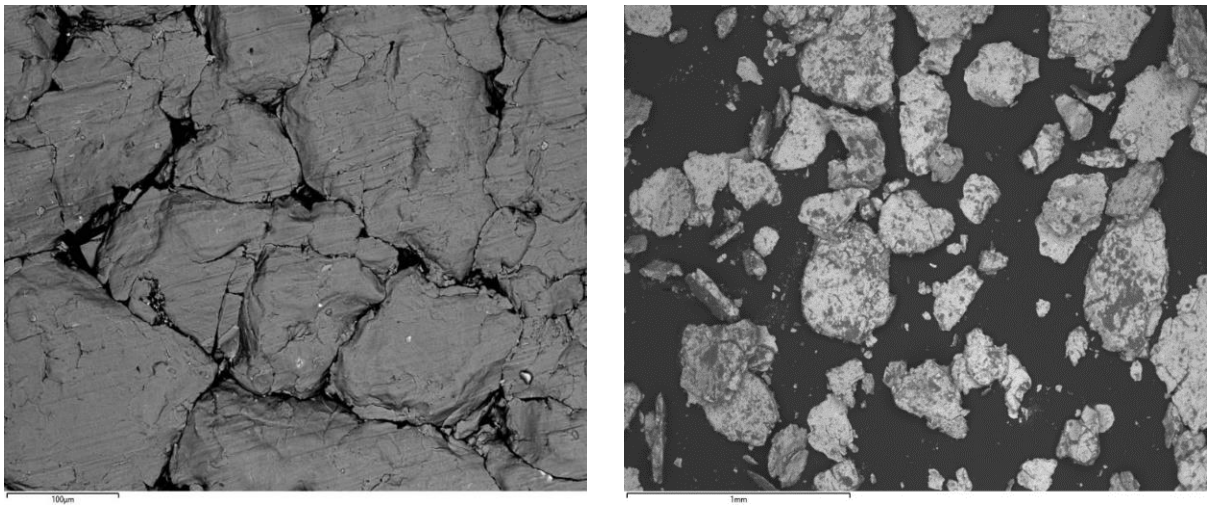

(**a**) (**b**)

Figure 2. Backscattered electron micrographs of (**a**) one-time cold-rolled $Ti_{16}V_{60}Cr_{24}$ alloy; (**b**) 5-min ball-milled $Ti_{16}V_{60}Cr_{24}$ alloy.

X-ray diffraction (XRD) patterns of as-cast $Ti_{16}V_{60}Cr_{24}$ alloys in various states are shown in Figure 3. All patterns show a BCC structure. Their crystal parameters are presented in Table 2.

We see that the differences of lattice parameters between the various states are small. The as-cast $Ti_{16}V_{60}Cr_{24}$ with and without Zr have similar crystallite size and microstrains but mechanical deformation by cold rolling or ball milling reduced the crystallite size.

For the alloy doped with 4 wt.% Zr, peaks corresponding to the secondary phase (seen in SEM micrographs) were expected. However, the XRD pattern only showed a pure BCC phase. As the phase fraction is quite low (only 7%), the Bragg peaks of this phase should have low intensities. Moreover, as the crystallite size of the BCC phase is quite small, the peaks are quite broad. Consequently, the combination of low peak intensities and their high width makes the secondary phase practically invisible in XRD spectra.

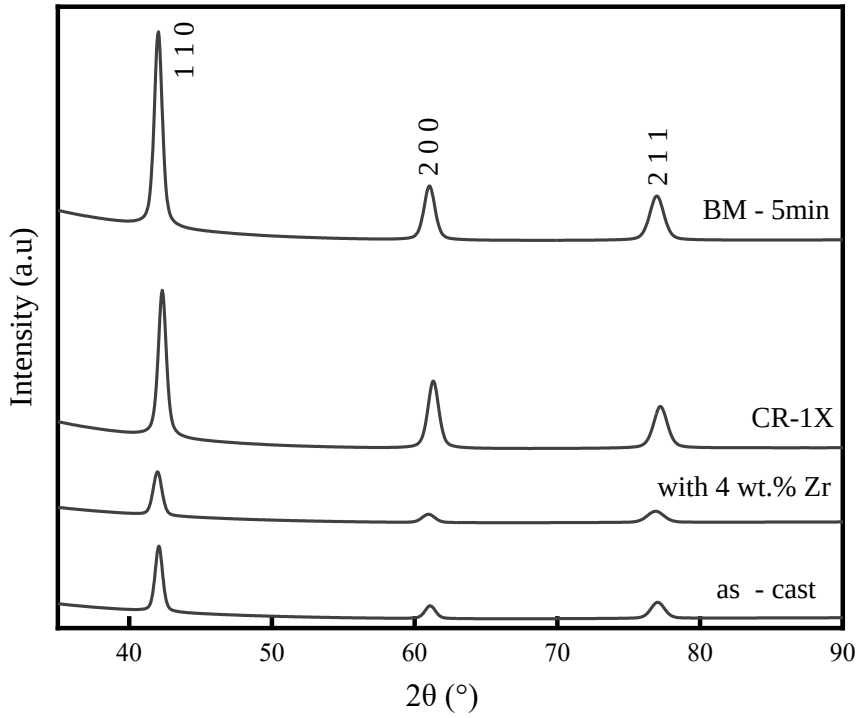

Figure 3. X-ray diffraction patterns of $Ti_{16}V_{60}Cr_{24}$ (with and without Zr addition) in various initial states.

Table 2. Crystal parameters of $Ti_{16}V_{60}Cr_{24}$ at various initial states. Numbers in parentheses are the error son the last significant digit.

Sample	Lattice Parameter (Å)	Crystallite Size (nm)	Microstrain (%)
as-cast	3.0295 (4)	36.1 (2)	1.08 (2)
with 4 wt.% Zr	3.0331 (6)	35.0 (2)	1.36 (2)
CR-1X	3.0325 (4)	26.2 (1)	1.02 (2)
BM-5 min	3.0310 (4)	28.1 (1)	1.05 (2)

3.2. First Hydrogenation

The kinetic curves of the first hydrogenation of all samples are shown in Figure 4. Each hydrogenation was performed at room temperature and under 3 MPa of hydrogen. The as-cast $Ti_{16}V_{60}Cr_{24}$ alloy showed a very slow absorption, reaching full capacity only after 26 h. Alloying with 4 wt.% of zirconium significantly improved the activation time. Full capacity was achieved after only 20 min. Both alloys attained the same maximum capacity of 3.8 wt.%. This value agrees with the calculated theoretical full capacity (H/M = 2 or 3.94 wt.%). As seen for similar systems, the enhanced kinetic of the alloy with zirconium is explained by the presence of a zirconium-rich secondary phase that acts as a gateway for hydrogen [20,23,24].

Better activation kinetics could also be achieved by mechanical deformation. As seen in Figure 4, ball milling or cold rolling of $Ti_{16}V_{60}Cr_{24}$ significantly improved the activation kinetics. The alloy that has been cold rolled once showed a fast kinetics, but a slightly reduced capacity compared to the unprocessed alloy. Ball milling for 5 min increased the kinetics, and the loss of capacity was minimal; however, it should be stressed that even though ball milling was for a very short duration, the whole process is much lengthier than cold rolling. Cold rolling was done in air, and, hence, the processing time was very short (just placing the powder between the steel plates and passing them between the rolls once). To perform ball milling, the crucible must be loaded in an argon-filled glove box. The crucible is then taken out of the glove box, installed on the milling machine and when

the milling is terminated, the crucible has to be reintroduced inside the glove box to unload it. Another advantage of cold rolling is that it could be performed in a continuous manner while ball milling is a batch process.

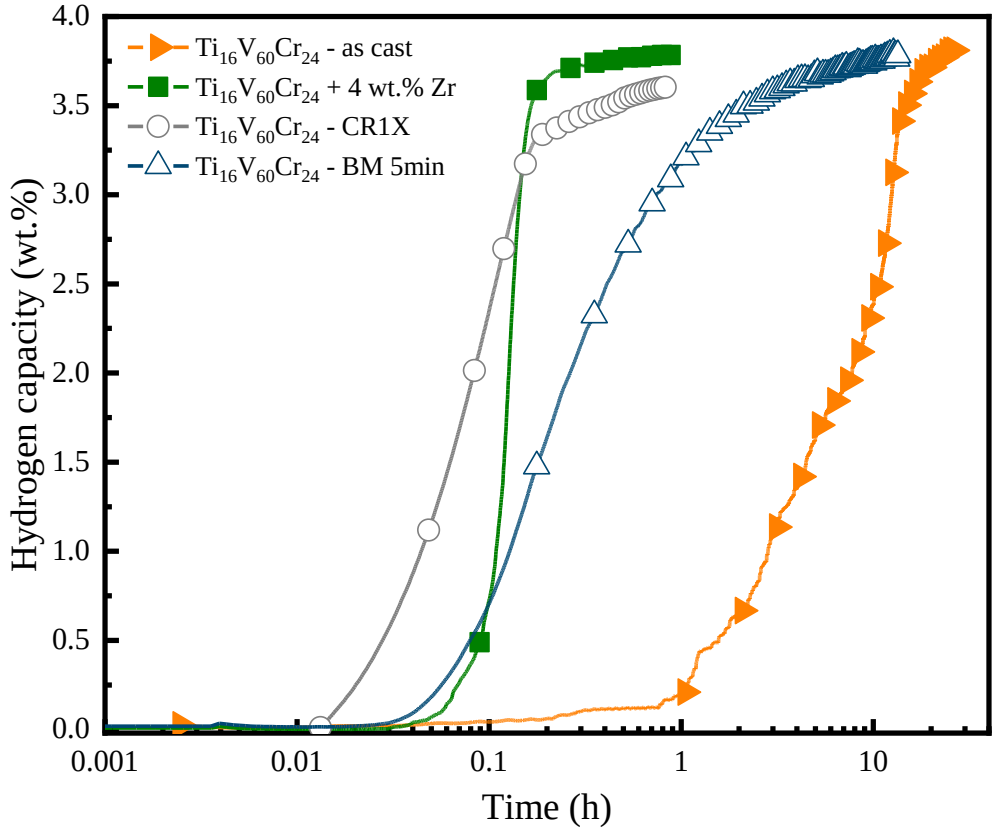

Figure 4. Activation curves of all samples at room temperature under hydrogen pressure of 30 bars.

The XRD patterns of the alloys after hydrogenation are shown in Figure 5. The hydrogenation transformed the BCC phase into a BCT structure for all alloys. Other unidentified peaks appear in all patterns. Since only one peak is unidentified in each XRD pattern, it is difficult to associate it with a particular crystal structure. Additionally, since the diffractograms were acquired in the air, the samples could partially desorb hydrogen and form oxides. The crystallographic parameters of activated samples are given in Table 3. We see that, for the BCT phase, the lattice parameter a is the same as the lattice parameter of the cubic phase in the as-received state while the c parameter is close to $a\sqrt{2}$.

Table 3. Crystal parameters of $Ti_{16}V_{60}Cr_{24}$ alloys after hydrogenation.

	Lattice Parameters (Å)	Crystallite Size (nm)	Microstrain (%)
as-cast	a = 3.0220 (3) c = 4.2408 (9)	12 (2)	—
+4 wt.% Zr	a = 3.0350 (2) c = 4.2640 (5)	40 (1)	1.09 (1)
CR-1X	a = 3.0258 (2) c = 4.2586 (4)	39 (5)	1.01 (2)
BM 5 min	a = 3.0136 (1) c = 4.2912 (2)	28 (3)	1.00 (1)

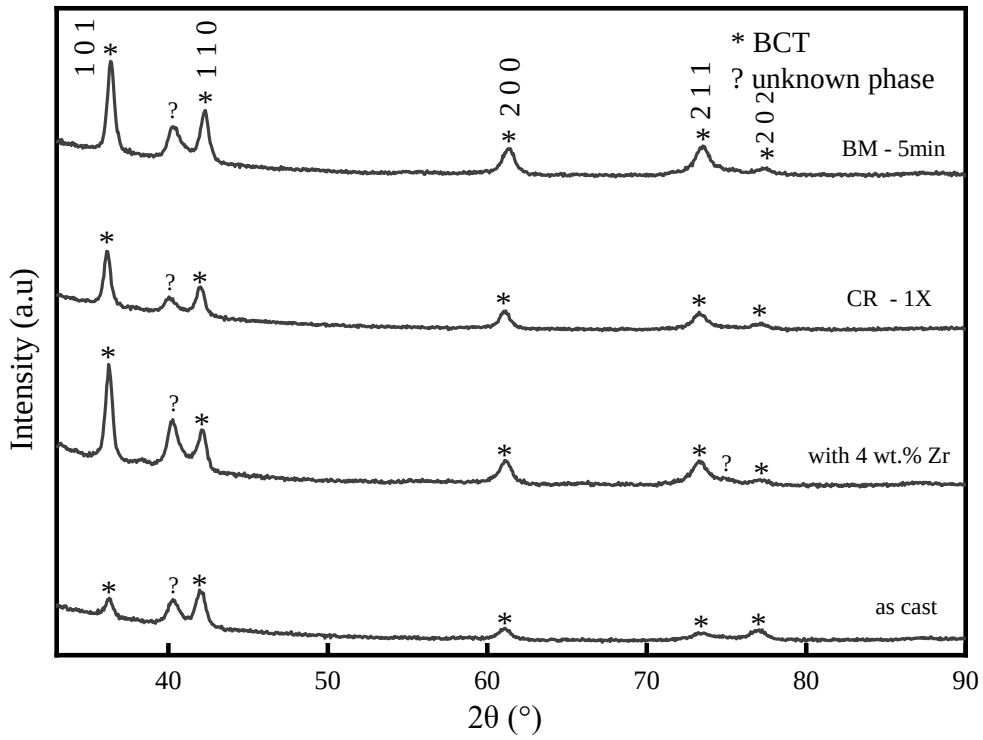

Figure 5. The XRD patterns of all studied $Ti_{16}V_{60}Cr_{24}$ alloys after hydrogenation (? is identified as the unknown phase).

3.3. Air Exposure Effect

For industrial production, it may be beneficial to have alloys that could be exposed to the air without losing their hydrogen storage properties. As the alloy with 4 wt.% Zr showed both good kinetics and high hydrogen storage capacity, we decided to study the effect of air exposure and subsequent cold rolling on it. Figure 6 shows the activation curves of $Ti_{16}V_{60}Cr_{20}$ + 4 wt.% Zr crushed in air and after different times of air exposure. The sample crushed in the air has practically the same incubation time (~1 min) as the sample crushed in argon, shown in Figure 4. It also has a good hydrogen capacity of 3.8 wt.%. After 1 day of air exposure, the incubation time is longer, the sample starts absorbing hydrogen after 65 min, but the hydrogen capacity remains 3.8 wt.%. To reduce this incubation time, one cold rolling pass has been done. That process shortens the incubation time to 3 min, but the hydrogen capacity slightly decreases to 3.7 wt.%. After 1 week of air exposure, the sample did not absorb hydrogen even after a few hours. However, cold rolling made the sample absorb in a few minutes but with a slight loss of capacity. For the sample exposed to the air for 1 month, one cold rolling pass was not sufficient to reach activation. However, five cold rolling passes resulted in an incubation time of about 20 min and total absorption of 3.4 wt.% of hydrogen in about 1 h.

3.4. PCI Curves of $Ti_{16}V_{60}Cr_{20}$ + 4 wt.% Zr

The thermodynamic properties of the alloy were determined by measuring the desorption pressure composition isotherms (PCI) at 298, 308 and 323 K. The corresponding Van't Hoff plot is presented in Figure 7. The matching pressures are chosen by considering the half-desorbed capacity (0.75 wt.%) of each PCI curve. The three PCI curves have the same shape and exhibit a sloping plateau. This is due to the random solid solution nature of the alloy which is associated with the distribution of the hydrogen binding energies in the interstitial sites. The desorbed capacity goes from 1.4 to 1.6 wt.% with increasing temperature. Knowing that those samples absorbed 3.8 wt.% of hydrogen means that between 2.2 and 2.4 wt.% of hydrogen is left in this compound. It closely corresponds to

the monohydride. The studied temperature range is small, but the pressure difference is noticeable. Thus, the thermodynamic parameters can be deducted.

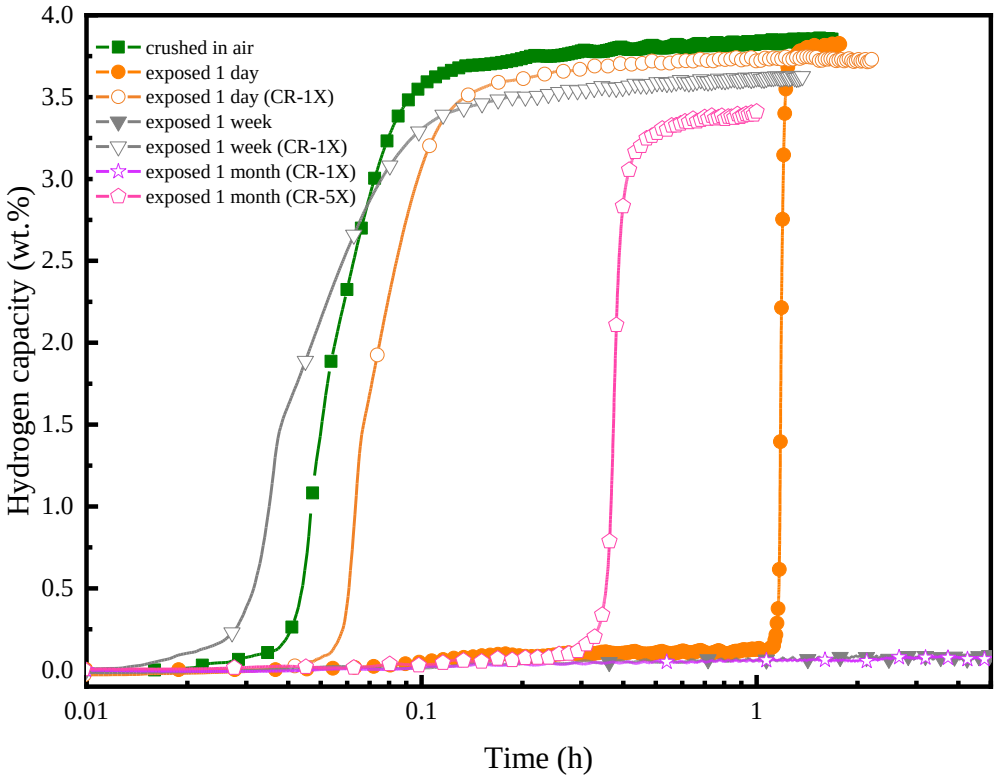

Figure 6. First hydrogenation at room temperature and 3 MPa of hydrogen of $Ti_{16}V_{60}Cr_{20}$ + 4 wt.% Zr alloy crushed in air and after different times of air exposure.

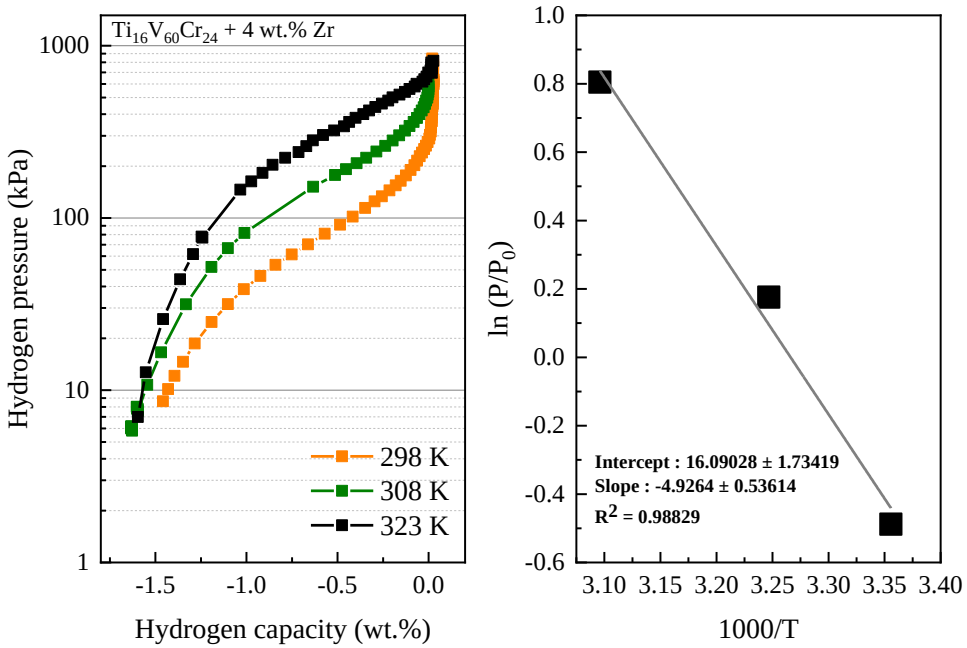

Figure 7. Desorption PCI curves of $Ti_{16}V_{60}Cr_{24}$ + 4 wt.%Zr at 298, 308 and 323 K.

The Van't Hoff plot gives the enthalpy and entropy values of (-41 ± 5) kJ/mol and (-134 ± 14) J/(mol·K), respectively. The isotherm at 323 K is similar to the one reported by Tamura et al. [25]. The entropy value of -41 kJ/mol is also in agreement with the one given by Kazumi et al. [2]. Compared to other vanadium-based ternary

alloys, such as $Ti_{0.1}V_{0.75}Mo_{0.15}$ (ΔH = 31 kJ/mol; ΔS = 130 J/(mol·K) and $(Ti_{0.1}V_{0.9})_{0.95}Cr_{0.05}$ (ΔH = 49 kJ/mol; ΔS = 138 J/(mol·K) [6], the enthalpy and the entropy tend to be in the same range. These values are also similar to the ones of the pure vanadium (ΔH = 40 kJ/mol; ΔS = 140 J/(mol·K) [26].

4. Conclusions

The following conclusions can be drawn from our study of the hydrogen storage properties of the vanadium-rich BCC $Ti_{16}V_{60}Cr_{20}$ alloy:

- The addition of 4 wt.% Zr is effective in improving the kinetics of the first hydrogenation of the alloy. It results in a fast absorption kinetic and a maximum hydrogen capacity of 3.8 wt.%.
- Air exposure results in an incubation time which increases with the air exposure time. Cold rolling helps regenerate the alloy by decreasing the incubation time, but it leads to a reduction of capacity.
- Enthalpy and entropy of hydride formation are -41 ± 5 kJ/mol -134 ± 14 J/mol/K, respectively.

Author Contributions: All experiments, except electron microscopy, were performed by F.R. under the supervision of J.H. J.H., E.R. and F.R. analyzed the results and wrote the paper. All authors have read and agreed to the published version of the manuscript.

Funding: This research received no external funding.

Institutional Review Board Statement: Not applicable.

Informed Consent Statement: Not applicable.

Data Availability Statement: Not applicable.

Acknowledgments: We would like to thank Agnes Lejeune for the electron microscopy experiments.

Conflicts of Interest: The authors declare no conflict of interest.

References

1. Kumar, S.; Krishnamurthy, N. Synthesis of V-Ti-Cr Alloys by Aluminothermy Co-Reduction of Its Oxides. *Process. Appl. Ceram.* **2011**, *5*, 181–186. [CrossRef]
2. Kazumi, T.; Tamura, T.; Kamegawa, A.; Takamura, H.; Okada, M. Effect of Absorption-Desorption Cycles on Structure and Stability of Protides in Ti-Cr-V Alloys. *Mater. Trans.* **2002**, *43*, 2748–2752. [CrossRef]
3. Dekhtyarenko, V.A.; Pryadko, T.V.; Savvakin, D.G.; Bondarchuk, V.I.; Mogylnyy, G.S. Hydrogenation Process in Multiphase Alloys of Ti-Zr-Mn-V System on the Example of Ti42.75Zr27Mn20.25V10 Alloy. *Int. J. Hydrogen Energy* **2021**, *46*, 8040–8047. [CrossRef]
4. Mazzolai, G.; Coluzzi, B.; Biscarini, A.; Mazzolai, F.M.; Tuissi, A.; Agresti, F.; Lo Russo, S.; Maddalena, A.; Palade, P.; Principi, G. Hydrogen-Storage Capacities and H Diffusion in Bcc TiVCr Alloys. *J. Alloys Compd.* **2008**, *466*, 133–139. [CrossRef]
5. Xiping, S.; Pei, P.; Peilong, Z.; Guoliang, C. Effect of Vanadium Content on Hydrogen Storage Property in Ti-V-Cr Alloys. *Rare Met.* **2006**, *25*, 374–377. [CrossRef]
6. Kumar, S.; Jain, A.; Ichikawa, T.; Kojima, Y.; Dey, G.K. Development of Vanadium Based Hydrogen Storage Material: A Review. *Renew. Sustain. Energy Rev.* **2017**, *72*, 791–800. [CrossRef]
7. Tsukahara, M.; Takahashi, K.; Mishima, T.; Isomura, A.; Sakai, T. Heat-Treatment Effects of V-Based Solid Solution Alloy with TiNi-Based Network Structure on Hydrogen Storage and Electrode Properties. *J. Alloys Compd.* **1996**, *243*, 133–138. [CrossRef]
8. Cho, S.W.; Yoo, J.H.; Chang, H.K.; Kim, W.B.; Kil, D.S.; Ahn, J.G. Changes in the Microstructure and Hydrogen Storage Properties of Ti-Cr-V Alloys by Ball Milling and Heat Treatment. *J. Alloys Compd.* **2011**, *509*, 5545–5550. [CrossRef]
9. Seo, C.Y.; Kim, J.H.; Lee, P.S.; Lee, J.Y. Hydrogen Storage Properties of Vanadium-Based b.c.c. Solid Solution Metal Hydrides. *J. Alloys Compd.* **2003**, *348*, 252–257. [CrossRef]
10. Miraglia, S.; De Rango, P.; Rivoirard, S.; Fruchart, D.; Charbonnier, J.; Skryabina, N. Hydrogen Sorption Properties of Compounds Based on BCC Ti 1-XV 1-YCr 1+x+y Alloys. *J. Alloys Compd.* **2012**, *536*, 1–6. [CrossRef]
11. Cho, S.W.; Han, C.S.; Park, C.N.; Akiba, E. Hydrogen Storage Characteristics of Ti-Cr-V Alloys. *J. Alloys Compd.* **1999**, *288*, 294–298. [CrossRef]
12. Yoo, J.H.; Shim, G.; Park, C.N.; Kim, W.B.; Cho, S.W. Influence of Mn or Mn plus Fe on the Hydrogen Storage Properties of the Ti-Cr-V Alloy. *Int. J. Hydrogen Energy* **2009**, *34*, 9116–9121. [CrossRef]
13. Huot, J.; Tousignant, M. Effect of Cold Rolling on Metal Hydrides. *Mater. Trans.* **2019**, *60*, 1571–1576. [CrossRef]

14. Sleiman, S.; Aliouat, A.; Huot, J. Enhancement of First Hydrogenation of Ti 1 V 0.9 Cr 1.1 BCC Alloy by Cold Rolling and Ball Milling. *Materials* **2020**, *13*, 3106. [CrossRef]
15. Lyu, P. Effect of Mechanical Deformation on Hydrogen Storage Properties of TiFe-Based Alloys. Ph.D. Thesis, Université du Québec à Trois, Rivières, QC, Canada, 2018.
16. Khajavi, S.; Rajabi, M.; Huot, J. Effect of Cold Rolling and Ball Milling on First Hydrogenation of Ti0.5Zr0.5 (Mn1-XFex) Cr1, X = 0, 0.2, 0.4. *J. Alloys Compd.* **2019**, *775*, 912–920. [CrossRef]
17. Shashikala, K.; Kumar, A.; Betty, C.A.; Banerjee, S.; Sengupta, P.; Pillai, C.G.S. Improvement of the Hydrogen Storage Properties and Electrochemical Characteristics of Ti 0.85 VFe 0.15 Alloy by Ce Substitution. *J. Alloys Compd.* **2011**, *509*, 9079–9083. [CrossRef]
18. Bibienne, T.; Razafindramanana, V.; Bobet, J.L.; Huot, J. Synthesis, Characterization and Hydrogen Sorption Properties of a Body Centered Cubic 42Ti-21V-37Cr Alloy Doped with Zr7Ni10. *J. Alloys Compd.* **2015**, *620*, 101–108. [CrossRef]
19. Dixit, V.; Huot, J. Investigation of the Microstructure, Crystal Structure and Hydrogenation Kinetics of Ti-V-Cr Alloy with Zr Addition. *J. Alloys Compd.* **2019**, *785*, 1115–1120. [CrossRef]
20. Sleiman, S.; Huot, J. Microstructure and Hydrogen Storage Properties of Ti1V0.9Cr1.1 Alloy with Addition of x Wt % Zr (x = 0, 2, 4, 8, and 12). *Inorganics* **2017**, *5*, 86. [CrossRef]
21. Bruker, A.X.S. TOPAS V3: General profile and structure analysis software for powder diffraction data. In *User's Manual*; Bruker AXS: Karlsruhe, Germany, 2005.
22. Yau, T.-L.; Annamalai, V.E. Corrosion of Zirconium and Its Alloys. *Ref. Modul. Mater. Sci. Mater. Eng.* **2010**, *3*, 2094–2134. [CrossRef]
23. Kamble, A.; Huot, J.; Sharma, P. Effect of Addition of Zr, Ni, and Zr-Ni Alloy on the Hydrogen Absorption of Body Centred Cubic 52Ti-12V-36Cr Alloy. *Int. J. Hydrogen Energy* **2018**, *43*, 7424–7429. [CrossRef]
24. Kamble, A. Effect of Additives, Heat Treatment and Mechanical Deformations on Hydrogen Storage Properties of BCC Alloys. Ph.D. Thesis, Université du Québec à Trois, Rivières, QC, Canada, 2018.
25. Tamura, T.; Kazumi, T.; Kamegawa, A.; Takamura, H.; Okada, M. Effects of Protide Structures on Hysteresis in Ti-Cr-V Protium Absorption Alloys. *Mater. Trans.* **2002**, *43*, 2753–2756. [CrossRef]
26. Reilly, J.J.; Wiswall, R.H. The Higher Hydrides of Vanadium and Niobium1. *Inorg. Chem.* **1970**, *9*, 1678–1682. [CrossRef]